0026-895X/92/010044-13$03.00/0

MOLECULAR PHARMACOLOGY, 42:44-56



# Molecular Neurotoxicology of Trimethyltin: Identification of Stannin, a Novel Protein Expressed in Trimethyltin-Sensitive Cells

STEPHANIE M. TOGGAS, J. KYLE KRADY,[1] and MELVIN L. BILLINGSLEY

*Department of Pharmacology, Pennsylvania State University College of Medicine, Hershey, Pennsylvania 17033*

Received December 19, 1991; Accepted April 3, 1992

**SUMMARY**

The molecular basis of selective vulnerability of specific neuronal populations to neurotoxicants remains a key focus in neurotoxicology. Trimethyltin (TMT) selectively damages neurons in rodent and human central nervous system after a single exposure. By coupling subtractive hybridization with molecular cloning techniques, we isolated a cDNA specifically localized in TMT-sensitive cells. This 2.9-kilobase cDNA encodes a putative 10-kDa peptide of 88 amino acids, termed "stannin." In immunocytochemical experiments, antisera raised against the amino terminus of stannin exhibited strong immunoreactivity in TMT-sensitive neurons in the hippocampus and entorhinal cortex, areas previously identified by *in situ* hybridization. Northern blot and *in situ* hybridization experiments detected a 3.0-kilobase stannin mRNA in brain, spleen, and kidney; expression occurred as early as embryonic day 15 in rat brain and thymus. *In situ* hybridization in human hippocampus demonstrated a stannin mRNA in pyramidal and dentate gyrus neurons. High stringency Southern blot analysis of genomic DNA identified stannin homologs in rabbit, *Drosophila*, and human. These findings indicate that stannin is present in TMT-sensitive cells and may play a role in the selective toxicity of organotin compounds.

The mechanisms responsible for selective cellular vulnerability to neurotoxicants may be as diverse as the cell types that comprise the CNS. In many cases, neurotoxicant actions are related to neuronal uptake and subsequent metabolic activation of neurotoxic compounds; both 1-methyl-4-phenyl-1,2,5,6-tetrahydropyridine and 6-hydroxydopamine are examples of such compounds (1). Recently, excitotoxic amino acids and their analogs have received considerable attention as agents that may cause selective neuronal loss (for review, see Ref. 2). In this case, cells that express excitotoxin receptors (e.g., *N*-methyl-D-aspartate, α-2-amino-3-hydroxy-5-methylisoxazole-4-propionate, and kainate receptors) are vulnerable to the actions of exogenous compounds that activate these receptors. An example of such a compound is domoic acid, a rigid structural analog of glutamate that has been linked to the recent outbreak of shellfish-induced neurotoxicity in eastern Canada (3).

Although mechanisms of selective vulnerability are known for some neurotoxicants, a widely divergent group of chemicals can cause damage to restricted areas of the CNS (4). It is difficult to predict, *a priori*, which compounds will cause selective toxicity and, further, which subtypes of cells will be affected by a given agent. Thus, there may be a broad range of target sites that render specific cell populations vulnerable to a given neurotoxicant.

The factors that predispose cells to the neurotoxic actions of heavy metals and organotin compounds are not well characterized. Organotin compounds are widely used as industrial catalysts and biocides, with several thousand tons of these agents being released into the environment annually (for review, see Ref. 5). Of the family of organotins, TMT and triethyltin cause neurotoxicity in a range of species, including humans. Triethyltin causes diffuse brain edema and damage of myelin. A single exposure to TMT, however, produces a specific pattern of neuronal loss in humans and rodents. Although limbic system structures such as hippocampus are extensively damaged,

This research was supported by United States Public Health Service Grant RO1-ES05450 and EPA Grant R818002-01-0 to M.L.B.

[1] Current address: Department of Neuropharmacology, Scripps Research Institute, La Jolla, CA 92037.

[2] Current address: Department of Human Genetics, Yale University School of Medicine, New Haven, CT 06510.

**ABBREVIATIONS:** CNS, central nervous system; TMT, trimethylin; SDS, sodium dodecyl sulfate; PAGE, polyacrylamide gel electrophoresis; ORF, open reading frame; KLH, keyhole limpet hemocyanin; E15, embryonic day 15; PND, postnatal day; PBS, phosphate-buffered saline; SSC, standard sodium/sodium chloride buffer; SSPE, standard sodium phosphate buffer; citrate bp, base pairs; kb, kilobases; RF, reading frame; HEPES, 4-(2-hydroxyethyl)-1-piperazineethanesulfonic acid; IPTG, isopropyl-β-D-thiogalactoside; Taq, *Thermus aquaticus*; MBP, maltose-binding protein; β-gal-α, β-galactosidase fusion protein.

damage occurs in other disparate regions of the CNS and peripheral nervous system (6). In addition, TMT is both nephrotoxic and lymphotoxic (7, 8).

Although the behavioral, electrophysiologic, and neuropathologic effects of TMT have been characterized, little is known concerning the mechanisms of TMT-induced toxicity. Several hypotheses originally centered around the uptake, distribution, and metabolism of TMT in neuronal tissues; however, a review of these data does not support a pharmacokinetic or metabolic explanation for TMT action. Because of the reliable pattern of damage produced by peripheral administration of TMT, this compound has been used as a model neurotoxicant for investigating changes subsequent to neuronal injury. Brock and O'Callaghan (9) have investigated changes in neurotypic and gliotypic proteins after TMT treatment, noting a transient loss of neurotypic proteins such as synaptophysin and synapsin in damaged regions such as hippocampus and limbic cortex. Neuronal loss was accompanied by robust increases in glial fibrillary acidic protein content, consistent with astrogliosis observed histologically (9, 10). Although quantitative changes in proteins may be useful indices of damage, these findings do not address the mechanisms of organotin toxicity.

In order to determine the mechanisms of TMT toxicity, we hypothesized that vulnerable cells expressed a gene product that sensitized them to the toxicant. To isolate such a gene product, we used avidin/biotin-based subtractive hybridization to obtain cDNAs representative of mRNAs expressed in sensitive cell populations (11). Using this approach, a cDNA fragment consisting of approximately 100 bp was isolated. This cDNA, designated p9T19, was used for Northern blot and *in situ* hybridization analysis. Preliminary results demonstrated that this cDNA recognized a 3.0-kb mRNA present in control but not in TMT-treated rat brain and that this mRNA was distributed in neuronal populations known to be sensitive to TMT. In order to characterize the gene product encoded by this differentially expressed cDNA, the p9T19 insert was used to screen a λZAP II rat brain cDNA library, with the goal of isolating a full-length clone. We now report the isolation of a full-length cDNA and the characterization of the gene product it encodes. This putative peptide has been named "stannin," from the Latin *stannum*, which means "related to tin."

## Materials and Methods

**cDNA probe preparation.** Plasmids containing partial cDNAs for stannin were isolated previously, using a rat brain cDNA fragment initially obtained by subtractive hybridization (11). The largest of these partial cDNA clones was termed pr9T19-I (referred to as I). In order to isolate a full-length clone, the 2.3-kb insert of the I clone was used as a probe for further library screens. The insert was isolated by digesting the plasmid with *Eco*RI (Promega) and electrophoresing the reaction on a 0.65% agarose gel in TAE (0.04 M Tris-acetate, 1 mM EDTA, pH 8.5) containing 0.5 μg/ml ethidium bromide. The insert band was excised from the gel, and the DNA was recovered as described (12). The insert was radiolabeled using [$\alpha$-$^{32}$P]dCTP (3000 Ci/mmol; Amersham) and a random hexamer priming kit, according to the instructions provided by the manufacturer (Promega). After chromatography on Sephadex G-50 (Pharmacia) to remove unincorporated nucleotides, the cDNA, in TE (10 mM Tris-HCl, pH 7.5, 1 mM EDTA, pH 8.0), was heat denatured and added directly to the hybridization solution. cDNA probes prepared in this manner were estimated, by liquid scintillation, to possess specific activities on the order of $10^9$ dpm/μg.

**cDNA library screening.** The full-length stannin cDNA was isolated by screening a λZAP II rat brain cDNA library (Stratagene) with the radiolabeled insert of the 2.3-kb I clone. Using the *Escherichia coli* strain XL1-Blue (Stratagene) as a host, the library was plated onto NZY medium (GIBCO) at a dilution that produced approximately 75,000 plaque-forming units/150-mm plate. Plaques were transferred to 0.45-μm nitrocellulose filters (BA85; Schleicher & Schuell), and filter lifts were performed in duplicate for each of 15 plates (total of $1.1 \times 10^6$ plaques screened). Filters were subjected to denaturing and neutralizing conditions as described (13), air dried, and baked for 1 hr at 80°, in a vacuum oven. Prehybridization was carried out for 2 hr at 62°, in a solution of 5× SSPE (diluted from 20× stock of 3 M NaCl, 0.2 M $NaH_2PO_4 \cdot H_2O$, 20 mM EDTA, pH 7.4), 2× Denhardt's solution, 0.1% SDS, and 150 μg/ml fragmented, denatured, salmon sperm DNA. Hybridization was performed for 24 hr at 62°, in fresh prehybridization solution containing the radiolabeled, heat-denatured, cDNA probe at a concentration of $2.1 \times 10^6$ dpm/ml. Filters were washed to a final stringency of 0.1× SSC/0.1% SDS, at 65° for 30 min. Autoradiography was performed on damp filters for 8–12 hr at −70°, with an intensifying screen, and plaques that produced a signal on both original and duplicate filters were cored into suspension medium (0.1 M NaCl, 8 mM $MgSO_4 \cdot 7H_2O$, 50 mM Tris, pH 7.5, 0.01% gelatin) plus chloroform. Secondary and tertiary screens of these positive plaques, plated at a lower density (approximately 100 plaque-forming units/100-mm plate), were carried out using the hybridization and washing conditions described above, so that well isolated, consistently positive plaques could be chosen for further analysis.

**Phagemid rescue procedure.** Plaques selected from each tertiary screen were cored into suspension medium plus chloroform, and an aliquot of the resulting phage stock, along with helper phage R408, was used to infect XL1-Blue *E. coli*. Phage particles were recovered in ampicillin-resistant bacterial colonies as recombinant pBluescript II $SK^{(-)}$ plasmids, according to the manufacturer's protocol (Stratagene). Individual colonies were used to inoculate LB broth containing 50 μg/ml ampicillin (Sigma), and minipreps of plasmid DNA were performed using standard methods (13).

**Selection of clones of interest.** Plasmids prepared as described above were digested with *Eco*RI and analyzed by agarose gel electrophoresis (0.7% agarose in 1× TAE plus 0.5 μg/ml ethidium bromide), to determine insert size. The gels were processed according to established protocols (13), and the plasmid DNA was vacuum transferred to Nytran (Schleicher & Schuell) in 10× SSC, to produce Southern blots. In addition, slot blots of alkali- and heat-denatured undigested plasmid DNA were prepared, and both slot blots and Southern blots were air dried and baked for 1 hr at 80° in a vacuum oven. The blots were prehybridized for 4 hr at 42° in a solution of 6× SSPE, 1% SDS, 10× Denhardt's solution, 20 μg/ml yeast tRNA, and 75 μg/ml fragmented, denatured, salmon sperm DNA. Three synthetic oligonucleotides chosen for identification of putative full-length clones were the following: FPI-1 (5′-dAGGCCCAGAAGCACGTGT-3′), located at the 5′ end of pr9T19-I; FP 4-3 (5′-dGGGAGGCAGATGCTAAGA-3′), located in the middle of the cDNA; and RP 2-3 (5′-dAGGTCAGTGGATGGTAGA-3′), located in a more 3′ region of the cDNA. These oligonucleotides were end-labeled with [$\gamma$-$^{32}$P]ATP (6000 Ci/mmol; Amersham), using bacteriophage T4 polynucleotide kinase (Promega), following standard protocols (13). Both Southern and slot blots were then hybridized for 24 hr in a solution of 6× SSPE/1% SDS, containing one of the three end-labeled oligonucleotide probes at a concentration of 1 pmol/ml. The hybridization temperature ($T_H$) was determined for each oligonucleotide probe (18-mer), using the following equation:

$$T_H = T_m - 5° = 2°(\text{A-T bp}) + 4°(\text{G-C bp}) - 5°$$

After hybridization, blots were washed to a final stringency of 0.1× SSPE/0.1% SDS, at the $T_H$ for 30 min. Autoradiography was performed on damp blots for 1–18 hr at −70°, with an intensifying screen. Subsequently, blots were stripped by washing for 1 hr at 68° in a solution of 70% formamide/6× SSPE, rinsed at room temperature in

2× SSPE, and rehybridized until all three probes had been hybridized to all blots. Plasmids of interest were selected based on insert size and hybridization profile, analyzed by restriction mapping using the enzymes *Bam*HI, *Hind*III, *Kpn*I, *Pst*I, *Sac*I, *Sal*I, *Xba*I, and *Xho*I (Promega), and purified by cesium chloride density gradient centrifugation, for further study.

**DNA sequencing.** Sequence determination was carried out via the dideoxy-nucleotide chain termination method (14), using Sequenase 2.0 (United States Biochemical) and Taq DNA polymerase (Promega) sequencing kits. The double-stranded template (4 μg) was denatured in 0.2 M NaOH, precipitated with ethanol, and resuspended in distilled water for sequencing reactions, which were performed using α-$^{35}$S-dATP (>1000 Ci/mmol; Amersham), following the instructions of the manufacturers. The ends of the clones were sequenced from the M13 forward and reverse primers present on the vector, flanking the insert; the remaining cDNA was sequenced using synthetic oligonucleotide primers (Hershey Medical Center Macromolecular Core Facility) generated to previously determined portions of the sequence. The full-length clone and several shorter clones were sequenced in their entirety from both strands of the template. In regions of high potential secondary structure, either dITP (United States Biochemical) or 7-deaza-dGTP (Promega) was substituted for dGTP in the Sequenase 2.0 or Taq DNA polymerase reactions, respectively. Reaction products were electrophoresed on 0.4-mm-thick, 6% polyacrylamide/7 M urea gels, in TBE (0.089 M Tris-borate, 2 mM EDTA, pH 8.0), at a constant voltage of 1600 V. The buffer system consisted of an upper buffer of 0.5× TBE and a bottom buffer of 1× TBE. Midway through electrophoresis, the bottom buffer was replaced with 1× TBE containing 3 M sodium acetate, to create a salt gradient for increased resolution of sequence information (15). After electrophoresis, gels were fixed for 25 min in 10% methanol/10% glacial acetic acid, mounted onto filter paper (Whatman 3MM), covered with plastic wrap, and dried at 80° for 2 hr on a vacuum dryer. After the plastic wrap was removed, autoradiography was performed for 12–18 hr at room temperature, with an intensifying screen, using either Kodak XAR or Kodak XRP film.

**Sequence analyses.** The nucleotide sequence of the full-length cDNA was analyzed by computer for potential ORFs, using the MacGene Plus package (Applied Genetic Technology, Inc.). The deduced amino acid sequence of the putative ORF was subsequently analyzed for relative hydrophilicity by using the Hopp-Woods algorithm, with a six-residue window (16). Using the FASTA search algorithm (17), the entire cDNA sequence of stannin (clone 37) was compared with the GenBank nucleotide sequence database, and the amino acid sequence of the stannin ORF was compared with the SwissProt and GenPept databases.

***In vitro* transcription.** For each of the five clones analyzed, the cesium chloride-purified pBluescript II SK(−) plasmid was linearized using two different restriction endonucleases, in two separate reactions. One reaction was performed using *Bam*HI, and the other was performed using *Sal*I; in experiments described above, these enzymes had been found not to digest the insert cDNA. After proteinase K digestion (Stratagene) and two phenol/chloroform (1:1) extractions, the linearized plasmids were precipitated with ethanol and resuspended in RNase-free TE. Approximately 1 μg of linearized plasmid was used in the *in vitro* transcription reactions. An mRNA-capping kit was purchased from Stratagene, and RNA containing a 5′meGppp5′G cap analog at the 5′ end was synthesized and purified according to the instructions provided. Two reactions were carried out for each clone, one using T7 bacteriophage RNA polymerase with the *Bam*HI-linearized template and one using T3 bacteriophage RNA polymerase with the *Sal*I-linearized template. For a positive control, a plasmid containing the ORF of SNAP-25 (18) was transcribed as described above and used in subsequent experiments.

***In vitro* translation.** Approximately 500 ng of the capped RNA transcript, synthesized as described above, were denatured at 67° for 10 min and added to a reaction system containing 17.5 μl of rabbit reticulocyte lysate (a gift from Dr. Keith Verner, Department of Cellular and Molecular Physiology, Hershey Medical Center), 20 μM amino acids minus methionine (Promega), and 30 μCi of [$^{35}$S]methionine (>1000 Ci/mmol; Amersham), in a total volume of 25 μl. After incubation for 1 hr at 30°, a 10-μl aliquot was added to 10 μl of SDS sample buffer (2% SDS, 10% glycerol, 0.1 M Tris·HCl, pH 6.8, 0.7 M 2-mercaptoethanol, 0.005% pyronin Y), and the mixture was electrophoresed on a 10–20% SDS-PAGE gradient (19). Gels were fixed for 20 min in a solution of 25% isopropanol/10% acetic acid, stained for 1 hr with 0.1% (w/v) Coomassie Brilliant Blue/50% methanol/10% glacial acetic acid, and destained overnight in 10% acetic acid/2% glycerol. Gels were incubated for 30 min with a fluorographic reagent (Amplify; Amersham), briefly rinsed in distilled water, covered with plastic wrap, and dried for 3 hr at 65° on a vacuum dryer. After the plastic wrap was removed, gels were exposed on X-ray film (Kodak XAR) for 19 hr at −70°, with an intensifying screen. A reaction containing brome mosaic virus mRNA (Promega) was used as a positive control, and a reaction containing no input mRNA was used as a negative control, to determine background levels of translation. These experiments used two separate lots of lysate, which differed slightly with respect to background but which had similar translation efficiency.

**Fusion protein production.** A protein fusion and purification system was purchased from New England Biolabs for production of stannin as a fusion protein in *E. coli*. The 2757-bp insert of clone 38 was blunt-ended with mung bean nuclease (Promega) and ligated to the *Stu*I-digested pMAL-c vector, so as to be in-frame with the coding sequence of MBP. The ligation mixture was used to transform competent TB1 *E. coli*, according to the instructions provided by the manufacturer. Recombinants were selected by means of a blue/white color screen (interruption of *malE-lacZα* gene fusion) on LB medium containing 100 μg/ml ampicillin, 80 μg/ml 5-bromo-4-chloro-3-indolyl-β-D-galactoside (Bethesda Research Laboratories), and 0.1 mM IPTG (Bethesda Research Laboratories). Plasmid minpreps were performed for selected white colonies; successful ligation of the clone 38 insert into the pMAL-c vector was confirmed and orientation was determined by restriction endonuclease digestion of plasmid DNA with *Pst*I. Colonies containing plasmids of interest were grown to an $A_{600}$ of approximately 0.5, and a 1-ml aliquot was removed. To induce expression of the MBP-stannin fusion protein, IPTG was added to the remaining cultures to a final concentration of 0.3 mM, and incubation was continued for 2 hr, followed by removal of a 0.5-ml aliquot. Uninduced and induced aliquots were microfuged, and pellets were resuspended in 50 μl and 100 μl of SDS sample buffer, respectively. Aliquots (15 μl) of each sample were electrophoresed on a 10% SDS-polyacrylamide gel, and proteins were visualized by staining of the gel with Coomassie brilliant blue.

**Experimental animals and tissue preparation.** Studies involving isolation of nucleic acids were carried out using adult male Long-Evans rats (200–500 g). Rats were anesthetized with sodium pentobarbital (50 mg/kg, intraperitoneally) and decapitated, and brains and other organs were quickly removed and frozen in liquid nitrogen. Tissues were stored at −70° until the time of the experiment.

For developmental experiments, a timed-pregnant colony of female Sprague-Dawley rats (200–250 g) was established, and gestational day 0 was determined as described previously (20). Pups (PND 1–12) were decapitated, and their brains were frozen in liquid nitrogen and subsequently stored at −70°. To obtain fetal tissue, E15 fetuses were removed surgically from anesthetized pregnant females (35–40 mg/kg sodium pentobarbital, intraperitoneally) and either dissected on ice for recovery of brains into liquid nitrogen or immersion-fixed in 4% (w/v) buffered paraformaldehyde in PBS, pH 7.4. Fixed embryos were then cryoprotected by incubation at 4° in a series of sucrose solutions (12%, 16%, 18%, 20%, and 25% sucrose in PBS), in preparation for sectioning.

Cytosolic and membrane fractions of rat hippocampus were prepared using adult male and female Sprague-Dawley rats. Rats were sacrificed by decapitation, brains were quickly removed, and hippocampi were dissected from fresh brains, on ice. Homogenization and centrifugation

to obtain samples for Western blot analysis were performed as described in the section on Western blot analysis.

Adult male Long-Evans rats (300–400 g) used for immunocytochemical studies were anesthetized with sodium pentobarbital (50 mg/kg, intraperitoneally) and perfused transcardially with PBS, followed by perfusion with freshly prepared 4% buffered paraformaldehyde in PBS. Brains were removed and cryoprotected in sucrose/PBS as described above.

For the studies using human brain tissue, a sample of human hippocampus was provided by Dr. Javad Towfighi (Department of Pathology, Hershey Medical Center). The sample was taken at autopsy, 21 hr after death, from a 72-year-old, white, female patient whose primary cause of death was acute necrotizing bronchopneumonia. Authorization and handling of the human autopsy sample were in accordance with guidelines established by the Department of Pathology, Hershey Medical Center. The sample was immersion-fixed in 10% neutral buffered formalin and was subsequently cryoprotected in sucrose/PBS, as described above.

**RNA isolation.** Total RNA was isolated from frozen rat peripheral tissues and whole rat brain by homogenization in 4 M guanidinium isothiocyanate (Bethesda Research Laboratories), followed by cesium chloride density gradient centrifugation (21). The RNA pellet was resuspended in 5 mM EDTA, pH 8.0, 0.5%, *N*-lauroylsarkosine, 5% 2-mercaptoethanol, extracted three times with phenol/chloroform/isoamyl alcohol (25:24:1), and precipitated with ethanol as described (15). This second RNA pellet was dried, resuspended in 0.5 ml of diethylpyrocarbonate (Sigma)-treated $H_2O$, and stored at −20°. Poly(A)$^+$ mRNA was isolated from the total RNA solution using poly(U) messenger affinity paper (Hybond-mAP; Amersham), as described by the manufacturer.

**Northern blot analysis.** Poly(A)$^+$ mRNA isolated from rat tissues and brains at different developmental stages was electrophoresed on 2.2 M formaldehyde-agarose gels (5 μg/lane). After electrophoresis, gels were processed according to established protocols (15), and the RNA was transferred to Nytran by capillary transfer, overnight, in 20× SSC. Duplicate gels were stained with ethidium bromide for visualization of the 18 S and 28 S rRNA species, to aid in molecular weight determinations and to enable detection of gross loading artifacts. The blots were air dried and baked for 1 hr at 80° in a vacuum oven. Prehybridization was carried out for 2 hr at 42°, in a solution of 50% formamide, 5× SSPE, 2× Denhardt's solution, 0.1% SDS, 10% dextran sulfate, and 100 μg/ml fragmented, denatured, salmon sperm DNA. Hybridization was carried out overnight at 42°, in fresh prehybridization solution containing the radiolabeled, heat-denatured, stannin cDNA probe at a concentration of $3 \times 10^6$ dpm/ml. Blots were washed to a final stringency of 0.1× SSC/0.1% SDS, at 55°, for 30 min. Autoradiography was performed on damp blots for 21 hr at −70°, with an intensifying screen. Blots were stripped by washing for 1 hr at 65° in a solution of 50% formamide/6× SSPE, rinsed at room temperature in 2× SSPE, and, as a control for equal loading of mRNA, rehybridized with an actin cDNA probe (22), using the same conditions as described above.

***In situ* hybridization.** For analysis of stannin mRNA expression in embryonic rat, fetuses were delivered by cesarean section on E15 and fixed as described above. Sagittal sections (20 μm) of whole embryos were cut on a cryostat at −20°, thaw-mounted onto gelatin/chromalum-coated microscope slides, and processed for *in situ* hybridization as described (23). Sections were hybridized with a [$\alpha$-$^{35}$S]UTP (>800 Ci/mmol; Amersham)-labeled stannin antisense RNA probe. Methods of probe preparation and purification, as well as conditions of prehybridization and hybridization, were as described previously (11). Sections were washed to a final stringency of 0.2× SSC, at 52°, for 30 min. Slides were air dried and autoradiographed for 2 days at room temperature, using Kodak XAR film. Slides of interest were emulsion-dipped using Kodak NTB-2 emulsion, exposed for 3 weeks, developed, and counterstained with cresyl violet.

For analysis of the hippocampal distribution of a human homolog of rat stannin mRNA, coronal sections (20 μm) of human hippocampus were prepared as described above. Hybridization and wash conditions were the same as those just described; however, it was necessary to increase the autoradiographic exposure time to 1–2 weeks. Selected slides were emulsion-dipped and processed as described above; however, exposure time was increased to 4–5 weeks.

**Antipeptide antisera production.** A 16-amino acid peptide of the sequence $H_2N$-Met-Ser-Ile-Met-Asp-His-Ser-Pro-Thr-Thr-Gly-Val-Val-Thr-Val-Cys-COOH was synthesized (Hershey Medical Center Macromolecular Core Facility) for use in production of antipeptide antisera in New Zealand White rabbits. The first 15 amino acids of this sequence correspond to those of the putative peptide specified by the stannin ORF. The cysteine residue at the carboxyl end was added for use in coupling the peptide, through the sulfhydryl group, to a carrier molecule, KLH (Sigma). The peptide-KLH conjugation was performed by first conjugating KLH to *m*-maleimidobenzoyl-*N*-hydroxysulfosuccinimide ester (Pierce) in 50 mM sodium phosphate, pH 7.4, purifying this conjugate by chromatography on Sephadex G-25 (PD-10; Pharmacia), and then adding it to an aqueous solution of the peptide (1.2 mg/ml). This mixture was incubated overnight, with shaking, at 4°. Approximately, 1 mg of the peptide-KLH conjugate was emulsified in Freund's complete adjuvant (GIBCO) and injected subcutaneously into each rabbit. Rabbits were injected biweekly, on four occasions, with 500 μg of the conjugate emulsified in Freund's incomplete adjuvant (GIBCO); subsequent injections consisted of 250 μg of conjugate emulsified in incomplete adjuvant, once every month. Rabbits were bled from the marginal ear vein 10 days after boosts, and serum was collected and stored in 20% glycerol at −20°.

**Western blot analysis.** Freshly dissected rat hippocampi were homogenized using a Teflon-glass pestle, in an ice-cold buffer of 20 mM HEPES, pH 7.4, 5 mM EDTA, containing 10 μM leupeptin (Sigma). After centrifugation at 1000 × *g* for 10 min at 4°, the pelleted material (P1 fraction) was discarded, and the supernatant (S1 fraction) was centrifuged at 30,000 × *g* for 30 min at 4°. The second pellet (P2 fraction) was resuspended in the homogenization buffer, and the protein content of the supernatant (S2 fraction) and the P2 fraction was determined by standard methods (20). Approximately 60 μg of protein from each fraction were added to SDS sample buffer and resolved on a 10–20% SDS-PAGE gradient (19). Proteins were transferred electrophoretically to 0.2-μm nitrocellulose membranes (BA83; Schleicher & Schuell), in a buffer of 25 mM Tris, 192 mM glycine, and 20% methanol. Blots were fixed for 20 min in a solution of 25% isopropanol/10% glacial acetic acid and were washed twice for 5 min in buffer A (50 mM Tris·HCl, pH 7.4, 150 mM NaCl, 1 mM $CaCl_2$). Nonspecific binding sites were blocked by incubating the blots in blocking solution (5% nonfat dry milk in buffer A) at room temperature for 1 hr or at 4° overnight. Preimmune sera and antipeptide antisera from bleeds three through seven were added to individual S2/P2 blots in blocking solution, at a dilution of 1/125, and were incubated overnight, with agitation, at 4°. After three 15-min washes in buffer A, blots were incubated for 2 hr, with agitation, at room temperature with an alkaline phosphatase-conjugated goat anti-rabbit IgG secondary antibody (Jackson ImmunoResearch Laboratories, Inc.), diluted 1/1000 in blocking solution. After three 15-min washes in buffer A, the blots were incubated with a 5-bromo,4-chloro,3-indoylphosphate, *p*-toluidine salt/nitroblue tetrazolium chloride (Amresco) chromagen system, as described previously (24), for visualization of immune complexes.

**Immunocytochemistry.** Adult rat brains were fixed and cryoprotected as described above. Coronal sections (20 μm) were cut on a cryostat at −20° and incubated overnight at 4° in buffer B [1% fatty acid-free bovine serum albumin (Sigma) and 0.3% Triton X-100 in buffer A]. Antipeptide antiserum was added in fresh buffer B, at a dilution of 1/250, and the sections were incubated for 24 hr at 4°. After three 10-min washes in buffer A, a secondary antibody, either fluorescein-conjugated or rhodamine-conjugated goat anti-rabbit IgG (Jackson ImmunoResearch Laboratories, Inc.), was added in buffer B, at a dilution of 1/500, and incubated with the sections for 2 hr at room temperature. After three 10-min washes in buffer A, sections were

A

B

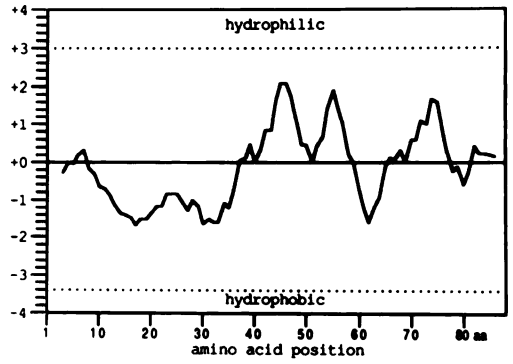


**Fig. 1.** cDNA and predicted amino acid sequences of stannin, and hydrophilicity analysis of the putative peptide. A, The nucleotide sequence of the full-length stannin cDNA was determined from both strands, as described in Materials and Methods. In addition, six independent overlapping cDNAs were sequenced and found to be identical to corresponding portions of the full-length clone. The consensus polyadenylation signal AAUAAA is found at positions 2800, 2860, and 2870. An ORF of 88 amino acids is predicted between nucleotides 148 and 411. The *underlined* portion of the amino acid sequence was used to specify a synthetic peptide for antisera production. B, Relative hydrophilicity of the putative stannin peptide. The amino-terminal region contains a large hydrophobic domain consisting of residues 10 through 35, followed by a relatively hydrophilic domain.

mounted onto microscope slides and provided with coverslips, using Gel/Mount mounting medium (Biomeda Corp.). Immune complexes were visualized via fluorescence microscopy on an Olympus BH-2 microscope. Photomicrographs were taken using Kodak Ektachrome 400 film.

**Genomic DNA isolation.** Genomic DNA was isolated from frozen whole rat brain and from SMS-KCNR human neuroblastoma cells (25) by lysis and digestion at 37° overnight, in a solution of 100 mM NaCl, 10 mM Tris·HCl, pH 8.0, 25 mM EDTA, pH 8.0, and 0.5% SDS, containing 0.1 mg/ml proteinase K (United States Biochemical), as described (15). Samples were extracted with phenol/chloroform/isoamyl alcohol (25:24:1) and precipitated with ethanol, and the DNA pellet was air dried and resuspended in TE, pH 8.0. *Drosophila* DNA was a gift from Dr. Paul Szauter (Department of Biological Chemistry, Hershey Medical Center), and rabbit spleen DNA was a gift from Dr. John Kreider (Department of Pathology, Hershey Medical Center).

**Southern blot analysis.** Samples of genomic DNA (10 μg), prepared as described above, were digested using either *Eco*RI or *Kpn*I. The reactions were carried out following standard protocols (13), and the DNA was precipitated with ethanol and resuspended in TE, pH 7.5. After addition of gel loading buffer to a final concentration of 0.04% bromophenol blue and 2.5% Ficoll, and incubation at 56° for 3 min, the mixtures were electrophoresed on a 0.65% agarose gel in 0.5× TBE containing 0.5 μg/ml ethidium bromide. After electrophoresis, the gel was processed according to established methods (13), and the DNA was vacuum transferred to Nytran in 10× SSC. The resulting blot was air dried and baked for 1 hr at 80° in a vacuum oven. Prehybridization was carried out for 2 hr at 42°, in a solution of 50% formamide, 5× SSPE, 2× Denhardt's solution, 0.1% SDS, 10% dextran sulfate, and 100 μg/ml fragmented, denatured, salmon sperm DNA. Stannin cDNA was radiolabeled with [$\alpha$-$^{32}$P]dCTP (Amersham), heat denatured, and added to fresh prehybridization solution at a concentration of $4.5 \times 10^6$ dpm/ml. Hybridization was performed at 42° overnight. The blot was washed to a final stringency of 0.1× SSC/0.1% SDS, at 65° for 30 min, and the damp blot was autoradiographed for 20 hr at −70°, with an intensifying screen, on Kodak XAR film.

**GenBank accession number.** The accession number for the sequence reported in this paper is M81639.

## Results

**Isolation of a full-length stannin cDNA.** In order to obtain a full-length cDNA, a series of cDNAs corresponding to the original p9T19 clone was isolated. The largest of these, a 2.3-kb cDNA termed p9T19-I, was used to screen a λZAP II rat brain cDNA library. Approximately $1.1 \times 10^6$ plaques were screened and, after secondary and tertiary screens were performed, 40 positive plaques were isolated. Phagemid rescue was carried out for recovery of the cDNAs as *Eco*RI inserts in pBluescript II SK(−) plasmids, and plasmids most likely to represent full-length clones were identified using the following strategy. Three synthetic oligonucleotides (18-mers), which spanned 5′, middle, and 3′ regions of the I cDNA, were selected from primers used in prior sequencing experiments. These primers were end-labeled with [$\gamma$-$^{32}$P]ATP and used to probe Southern blots containing *Eco*RI-digested plasmid DNA of each clone. These same probes were used to analyze slot blots

of undigested plasmid DNA of the 40 clones. In every case, the pattern of hybridization obtained on slot blots was consistent with that obtained on Southern blots (data not shown).

Clones were classified according to the hybridization profiles generated by the three oligonucleotides. Of the 40 clones isolated, eight were classified as 5′ clones (those recognized by the 5′ and middle primers but not the 3′ primer), 13 were classified as 3′ clones (those recognized by the middle and 3′ primers but not the 5′ primer), and 17 were classified as clones containing 5′, middle, and 3′ regions of the I clone (those recognized by all three primers). Two clones were not recognized by any of the primers and were omitted from further study. A total of 25 clones hybridized to the 5′ primer; both restriction analysis and sequencing revealed that these clones aligned with each other and that the largest of these were likely to represent a full-length cDNA.

Within each group, clones were classified on the basis of insert size. Sizes ranged from 1.1 to 3.5 kb. Because the original p9T19 cDNA recognized a 3.0-kb mRNA species on Northern blots of brain poly(A)$^+$ mRNA (11), clones of interest were those with inserts in this size range. The largest clones in each of the three groups were analyzed by restriction endonuclease digestion using eight different enzymes; restriction maps of these clones were compared with those obtained for I and smaller clones isolated previously. Restriction analysis resulted in the elimination of two of the clones from further study, because they were found to possess head-to-head ligated repeats of their cDNA sequences and, thus, to represent cloning artifacts. Of the remaining clones, those that possessed the largest inserts were those that hybridized to all three oligonucleotide probes. Several of these clones displayed restriction maps similar to I; they differed from I only in their 5′ ends, which were larger, containing an extra *Pst*I site. These observations indicated that such clones were likely to be larger representations of I and that the newly cloned information resided in the 5′ end. Because these clones were most likely to contain the ORF start site, they were purified by cesium chloride density gradient centrifugation, for subsequent sequence analysis.

Initial sequence analysis using the M13 forward and reverse primers flanking the insert revealed clones that possessed a 3′ poly(A) tail and new 5′ information. Three of these clones, 14, 37, and 38, were sequenced in their entirety, using both strands of the cDNA as templates. The largest clone (clone 37) was determined to be 2912 bp in length, terminating in a poly(A) tail that was preceded by three AAUAAA consensus polyadenylation signals (bp 2800–2805, bp 2860–2865, and bp 2870–2875); the sequence of this clone is shown in Fig. 1A. Analysis for potential protein-coding regions revealed a putative ORF in the 5′ end, extending from position 148 to position 411. Two in-frame stop codons (bp 31–33 and bp 94–96) were found upstream of the putative translation initiation site, suggesting that the entire 5′ end of the coding region was contained within this cDNA. This initiation site is surrounded by the sequence GCACTGACCATGT (bp 139–151), which is similar to the consensus sequence for initiation of translation (26). The peptide predicted by the ORF, termed stannin, consists of 88 amino acids; the deduced amino acid sequence of this peptide is shown in Fig. 1A, using the three-letter code for amino acids. Several additional clones that contained this putative ORF were found to be identical in sequence throughout the coding region.

Hydrophilicity analysis of the putative stannin peptide was performed using the Hopp-Woods algorithm and indicated that a hydrophobic domain of 25 residues was present in the amino terminus (Fig. 1B). The rest of the peptide was found to be largely hydrophilic.

The nucleotide sequence of the full-length stannin cDNA (clone 37) was compared with the sequences contained in the GenBank database; however, no homologies were found to any portion of the cDNA. Likewise, searches of the SwissProt and GenPept protein databases failed to reveal any significant homologies to the deduced stannin amino acid sequence. As a result of these findings, it was concluded that stannin represents a novel gene product.

***In vitro* translation analysis of stannin clones.** To verify the identity of the putative ORF, selected clones were analyzed for the ability to synthesize the predicted translation product *in vitro*. Sense and antisense mRNAs containing a 5′ cap structure were synthesized for selected clones, using the T7 and T3 bacteriophage RNA polymerase promoters flanking the insert on the pBluescript II SK(−) plasmid. For *in vitro* translation analysis, these synthetic mRNAs were added to a rabbit reticulocyte lysate system, along with [$^{35}$S]methionine. Fig. 2A shows results obtained for five independent clones. Fig. 2B illustrates a partial restriction map and compares, with respect to each other and to the ORF, the alignment of these and other

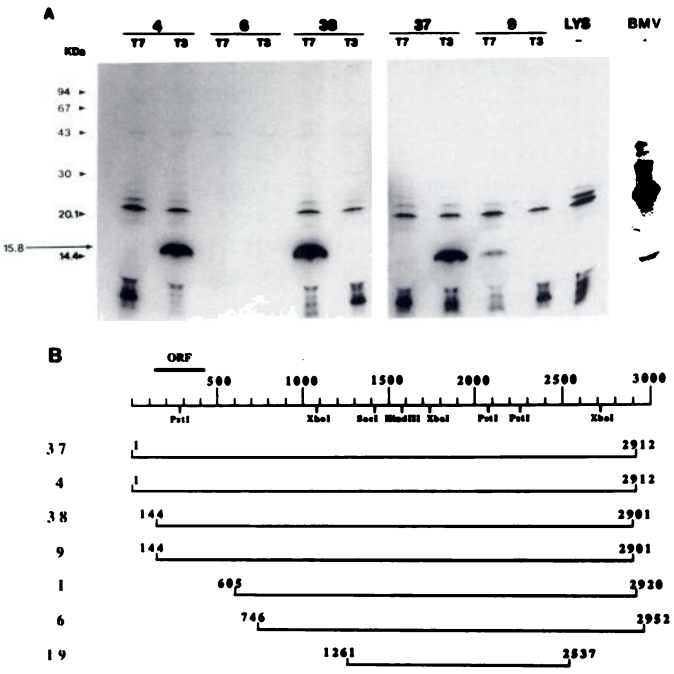


**Fig. 2.** *In vitro* transcription and translation of stannin cDNAs. A, RNA was transcribed from five independent stannin/pBluescript II SK(−) plasmids and added to a rabbit reticulocyte lysate system containing [$^{35}$S] methionine as a label. *In vitro* translation products were resolved on SDS-PAGE gradients (10–20%) and detected using fluorography. Clones 4, 38, 37, and 9 generated a peptide that migrated at 15.8 kDa (*arrow*). In each case, the antisense strand failed to generate a product. Clone 6, which does not contain the putative ORF, did not generate this peptide. *LYS*, no input mRNA (negative control); *BMV*, brome mosaic virus mRNA (positive control). B, Partial restriction map of stannin cDNAs, and alignment showing the putative ORF. Clones I (data not shown) and 6, which do not contain the putative ORF, failed to generate an *in vitro* translation product. Clone 19 represents the pr9T19 clone isolated previously (11); this clone was not analyzed by *in vitro* translation but is included to illustrate its alignment relative to the full-length cDNA. The additional 3′ information in clones I and 6 represents their longer poly(A) tracts.

clones, I and 19, isolated previously. In reactions containing the sense strand mRNA, all clones whose cDNAs spanned the ORF, 4, 38, 37, and 9, produced a translation product with an apparent mobility of 15.8 kDa. Reactions containing the antisense strand did not produce this product. Because of the random nature of the orientation of inserts within the vector, the sense strand of some clones was produced using the T7 promoter, whereas that of others was produced using the T3 promoter. Orientation was confirmed by sequence analysis. Clone 6 did not produce a translation product, and, as diagrammed in Fig. 2B, its cDNA does not contain the region of the putative ORF; the same was true for the I clone (data not shown).

As a positive control for both transcription and translation, a plasmid containing the ORF of SNAP-25 (18) was transcribed from both promoters, and the sense and antisense mRNAs generated were used in *in vitro* translation reactions. Only translation of the sense mRNA produced the 25-kDa protein (data not shown). A reaction containing no input mRNA was included as a negative control; this result illustrated background levels of translation of mRNAs endogenous to the lysate and identified nonspecific translation products. The batch of lysate used to translate clone 6 possessed a lower background than did the other batches of lysate but was equally effective in translating mRNA (data not shown). Brome mosaic virus mRNA was included as a positive control for translation.

**Expression of stannin as a fusion protein in *E. coli*.** Large quantities of a MBP/stannin fusion protein were produced by subcloning the insert of clone 38 into the pMAL-c bacterial expression vector (Fig. 3A). Clone 38 was chosen because its 5′ end is very close to the ORF start site, facilitating in-frame insertion and minimizing the amount of 5′-untranslated sequence to be incorporated into the fusion protein amino acid sequence. After blue/white colony selection, identification of recombinant plasmids was verified by restriction analysis. Expression was induced by IPTG, and the protein produced was analyzed by SDS-PAGE, as shown in Fig. 3B. This fusion protein was estimated to be 52 kDa (Fig. 3B, *lane 2*). The molecular mass of MBP alone is 42 kDa (Fig. 3B, *lane MBP*); thus, the mobility of the induced protein in Fig. 3B, *lane 2*, was consistent with a fusion between the 10-kDa stannin peptide and the 42-kDa MBP. A vector containing the insert in the reverse orientation produced only MBP upon induction with IPTG (Fig. 3B, *lane 3*), consistent with the absence of a viable in-frame ORF. The protein induced from a nonrecombinant plasmid, MBP/β-gal-α, is shown in Fig. 3B, *lane 1*; this fusion protein also migrates as a 52-kDa peptide. Partial proteolytic digestion of the MBP/β-gal-α and the MBP/stannin fusion proteins with *Staphylococcus aureus* V8 protease verified that the stannin fusion was a different peptide than the MBP/β-gal-α fusion (data not shown). In addition, digestion with *Pst*I had demonstrated that the plasmid encoding the MBP/stannin fusion protein contained the stannin cDNA, although that encoding the MBP/β-gal-α fusion protein did not. Thus, two different plasmids produced two different fusion proteins of similar molecular mass. When vectors were digested with *Pst*I, a cDNA insert was observed only in digests of the in-frame stannin plasmid and not for the reverse orientation, further demonstrating that the fusion protein was expressed in an orientation-specific mode. These results indicate that the putative stannin ORF encodes a protein of ~10 kDa, as predicted

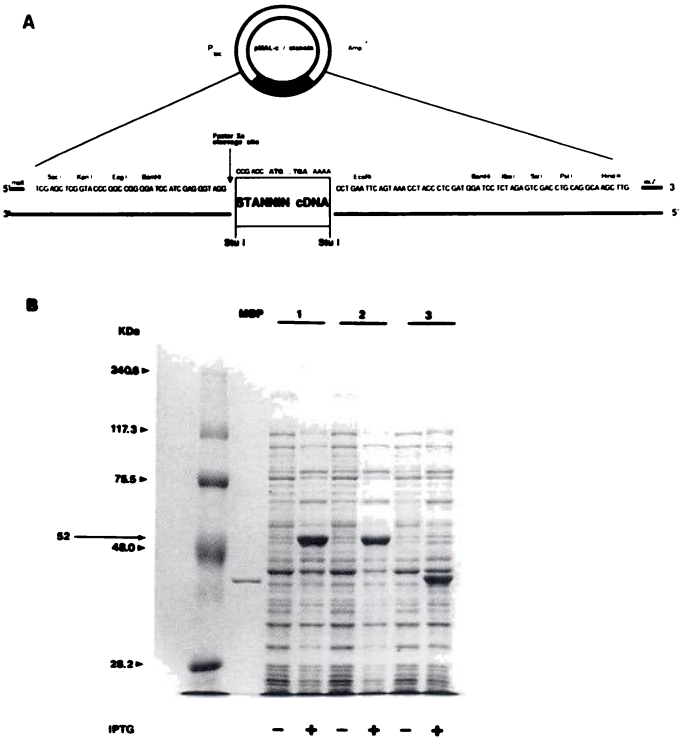


**Fig. 3.** Expression of stannin as a fusion protein in *E. coli*. A, Map of stannin cDNA subcloned into the pMAL-c bacterial expression vector (New England Biolabs) for production of the protein encoded by the putative ORF. Recombinants were selected by means of a blue/white color screen (interruption of *malE-lacZα* gene fusion) and restriction analysis. B, Induction of expression by IPTG. Uninduced and induced aliquots were electrophoresed on a 10% SDS-polyacrylamide gel, and proteins were visualized by staining of the gel with Coomassie Brilliant Blue. The vector containing the insert in the correct orientation (*lane 2*) shows induction of a protein of approximately 52 kDa, which is consistent with fusion of a 10-kDa protein to the 42-kDa MBP. The vector containing the insert in the reverse orientation (*lane 3*) shows induction of the MBP only. *Lane MBP*, purified MBP (supplied by manufacturer); *lane 1*, vector only (no insert; induction of MBP-β-gal-α fusion); *lane 2*, vector plus insert (correct orientation); *lane 3*, vector plus insert (reverse orientation).

by sequence analysis and as suggested by *in vitro* translation results.

**Northern blot analysis.** To assess the tissue specificity of stannin mRNA expression, Northern blot analysis of size-fractionated poly(A)$^+$ mRNA from several rat tissues was carried out using a radiolabeled stannin cDNA probe. As shown in Fig. 4A, this probe hybridized to an mRNA species of approximately 3.0 kb in kidney and spleen. A stronger signal was obtained in spleen, suggesting that the transcript is present at higher levels in this tissue. In liver, heart, and testes, the probe did not recognize the 3.0-kb stannin mRNA, or any others. Therefore, expression of stannin mRNA appears to be under tissue-specific regulation.

The developmental pattern of stannin mRNA expression in rat brain was investigated by using this same cDNA as a probe for Northern blots containing poly(A)$^+$ mRNA from whole brains from rats of developmental ages E15, PND 1, 5, 12, and 20 or from adult rats (Fig. 4B). A single mRNA species of 3.0 kb was detected at all ages, with the strongest signal seen in the adult. After these experiments, both blots in Fig. 4 were hybridized with a radiolabeled chicken β-actin cDNA, to verify that equal amounts of RNA were present in each lane (data not shown).

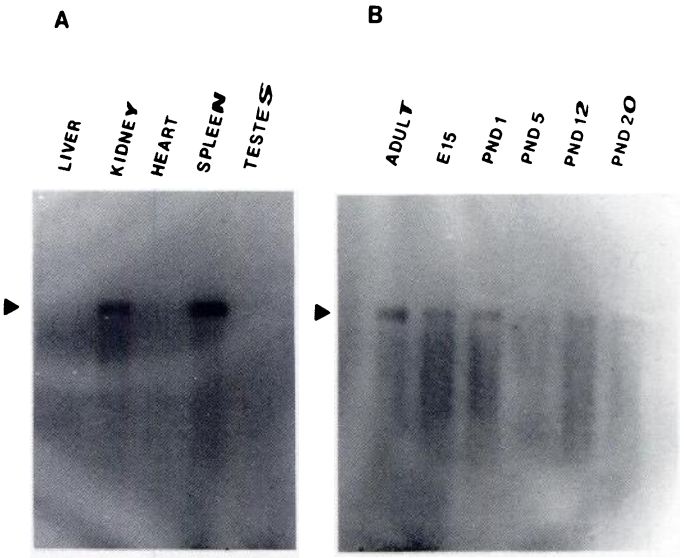


**Fig. 4.** Northern blot analysis of stannin mRNA expression in rat tissue and during rat brain development. Poly(A)$^+$ mRNA was isolated from various tissues and from brains at different developmental stages, electrophoresed, and blotted onto nylon, as described in Materials and Methods. Stannin cDNA was radiolabeled with [$\alpha$-$^{32}$P]dCTP and hybridized to the Northern blots. Blots were stripped and rehybridized with a [$\alpha$-$^{32}$P]dCTP-labeled chicken $\beta$-actin cDNA, as a control for equal loading of samples (data not shown). A, Hybridization of stannin cDNA to mRNA in peripheral tissues. Hybridization to a 3.0-kb mRNA species present in both kidney and spleen was observed (*arrowhead*); no detectable hybridization was observed to mRNA isolated from liver, heart, or testes. B, Hybridization of stannin cDNA to a 3.0-kb mRNA present in brain; hybridization was observed from E15 through adult (*arrowhead*).

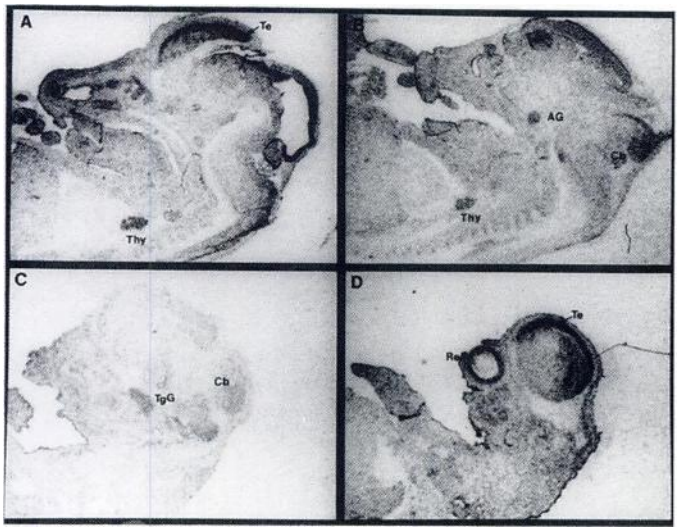


**Fig. 5.** Pattern of *in situ* hybridization of stannin antisense RNA in embryonic rat. *In situ* hybridization was performed on sagittal sections (20 $\mu$m) of rat embryos (E15), using radiolabeled stannin antisense RNA, as described in Materials and Methods. Sections were exposed to X-ray film for 2 days. Each panel represents an autoradiographic image of the head and chest of E15 rats, progressing from midline in A to the most lateral section in D. *Te*, telencephalon; *Thy*, thymus; *AG*, autonomic ganglion; *Cb*, cerebellum; *TgG*, trigeminal ganglion; *Ret*, retina.

***In situ* hybridization analysis of stannin mRNA expression in embryonic rat.** The expression of stannin mRNA in the developing rat was localized by hybridizing a radiolabeled stannin antisense mRNA probe to 20-$\mu$m sagittal sections of E15 rat embryos. The midline section in Fig. 5A shows intense hybridization in the telencephalon and thymus. The more lateral sections in Fig. 5, B–D, reveal stannin expression in the autonomic ganglion, cerebellum, and trigeminal ganglion. Intense hybridization was also detected in embryonic retina (Fig. 5D). Adjacent sections were hybridized with a stannin sense RNA probe, as a control to determine background levels of hybridization; this probe did not show specific hybridization to any regions of the embryos (data not shown).

**Identification and localization of the stannin peptide in rat brain.** Antisera recognizing the native stannin peptide were generated in rabbits, using a synthetic peptide corresponding to the first 15 residues of the stannin amino-terminal sequence (underlined in Fig. 1A). The peptide contained a carboxyl-terminal cysteine, enabling it to be specifically conjugated to a carrier immunogen, KLH. Rabbits were injected and bled according to the schedule outlined in Materials and Methods. Sera from each bleed were screened for ability to detect a protein in the appropriate molecular mass range (10–15 kDa) on Western blots of membrane and cytosolic fractions of rat hippocampus. As shown in Fig. 6A, the crude antisera detected a protein of 10-kDa in hippocampal cytosol. No immunoreactivity was detected on similar blots incubated with a preimmune sera (Fig. 6B). Additional high molecular mass peptides were detected by the crude antisera, suggesting that either the stannin epitope or an epitope from KLH may be present on other proteins.

To examine the regional localization of the stannin peptide in adult rat brain, coronal sections (20 $\mu$m) were incubated with the stannin antipeptide antisera, and immune complexes were visualized using either fluorescein- or rhodamine-conjugated secondary antibodies. Specific punctate immunofluorescence was observed in all hippocampal pyramidal cell fields. Fig. 7A depicts stannin immunofluorescence in Ammon's horn; Fig. 7B shows a higher powered view of CA3 pyramidal cells, detailing the punctate and primarily somatic localization of the signal. Immunoreactivity was absent from mossy fibers. Fig. 6, C and D, shows immunoreactivity in CA1 pyramidal cells and in the

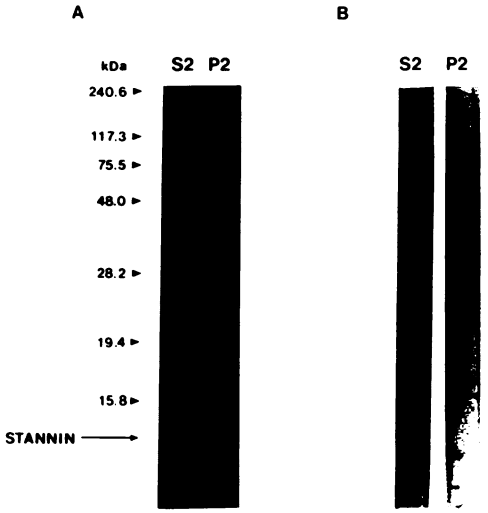


**Fig. 6.** Western blot analysis of stannin in rat brain. A, Membrane and cytosolic fractions of rat hippocampus were resolved by SDS-PAGE on a 10–20% gradient and were blotted to nitrocellulose. The blot was incubated with antiserum against a KLH conjugate of residues 1–15 of stannin, at a 1/125 dilution, and immunoreactivity was detected using an alkaline phosphatase-linked secondary antibody (1/1000). Among the proteins recognized is a 10-kDa cytosolic protein (*arrow*), which is consistent with the size of the peptide predicted by the putative ORF. B, Preimmune sera failed to recognize any peptides.

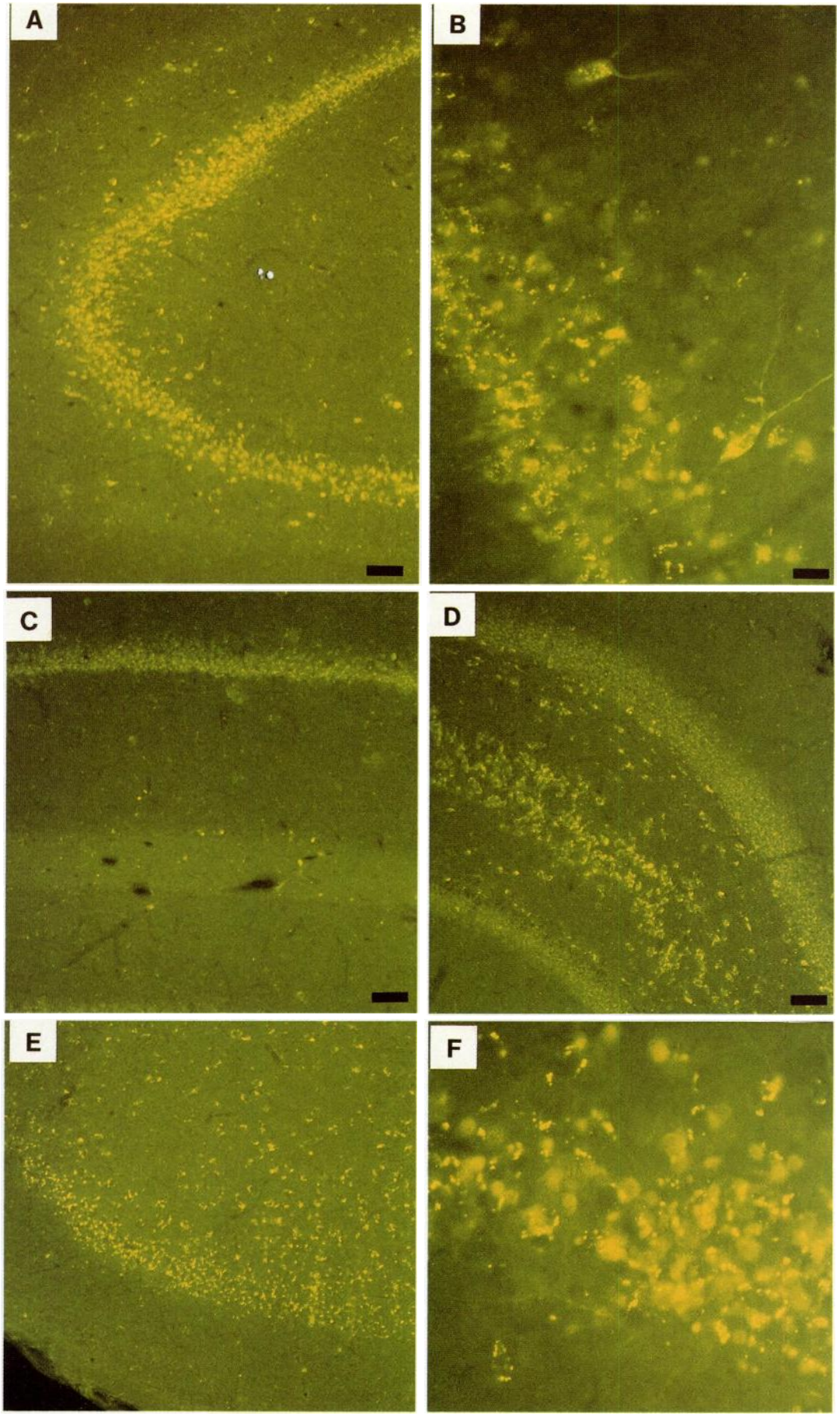


**Fig. 7.** Immunocytochemical localization of stannin in rat brain. Coronal sections (20 $\mu$m) of rat brain were incubated with antipeptide antiserum at a 1/250 dilution, and immunoreactivity was detected using a fluorescein-conjugated secondary antibody (1/500). Fluorescence microscopy was used to visualize immune complexes. A, Immunoreactivity in Ammon's horn of the hippocampus (100×) (*bar* = 100 $\mu$m), showing punctate somatic

dentate gyrus and hilus. Again, immunoreactivity was confined to the soma and was punctate. Fig. 7, E and F, demonstrates that stannin immunofluorescence was observed in layers 2 and 3 of the entorhinal cortex. Staining of layer 2 stellate cells was, again, somatic and punctate. Immunoreactivity was restricted to specific, TMT-sensitive cell types in hippocampus, neocortex, and other brain regions. This pattern of peptide immunolocalization paralleled the localization of stannin mRNA determined using *in situ* hybridization (11).

**Detection of a stannin mRNA homolog in human hippocampus.** Because human hippocampal cells are damaged by TMT, we used *in situ* hybridization analysis to determine whether these cells expressed an mRNA species homologous to that of rat stannin. A sample of human hippocampus was obtained at autopsy from a patient who died of non-neurological causes, as detailed in Materials and Methods. Tissue was fixed, and coronal sections (20 μm) were hybridized with a radiolabeled stannin antisense RNA probe. The autoradiograph in Fig. 8A shows the pattern of hybridization obtained with this probe (4× magnification). Hybridization was detected in the pyramidal cell bodies of the hippocampal fields and in the granule cells of the dentate gyrus; this pattern was similar to that seen previously in rat hippocampus (11). The punctate nature of the signal in these areas can be seen via dark-field microscopy of emulsion-coated sections, at higher magnifications (Fig. 8, B–D). Although the intensity of hybridization was much weaker than in rat, as evidenced by the longer exposure times required for signal detection, the similarity of specificity and pattern of hybridization between rat and human indicated that sequence homology exists between these mRNAs.

**Southern blot analysis.** The discovery of an mRNA homologous to stannin in human brain prompted investigation of species distribution of putative stannin-related genes. Southern blot analysis of restriction endonuclease-digested genomic DNA from *Drosophila*, rabbit, rat, and human was performed, using a radiolabeled stannin cDNA probe. Results of this analysis are shown in Fig. 9, where strong hybridization to genomic DNA occurred in all species analyzed. Equal loading of DNA was confirmed by staining of the gel with ethidium bromide before transfer (data not shown). The signal was obtained after a high-stringency wash with 0.1× SSC/0.1% SDS for 30 min at 65°. These observations suggest that a strong homology exists between the stannin probe and its target DNA, and they indicate that conservation of the stannin gene may exist among species.

## Discussion

A full-length rat brain cDNA clone whose gene products localize in cells that are sensitive to TMT has been isolated and characterized. This novel cDNA contains a 264-bp ORF that predicts an 88-amino acid peptide, termed stannin. For the following reasons, we have concluded that this clone represents a full-length cDNA. 1) The size of the cDNA, 2.9 kb, corresponds closely to the 3.0-kb mRNA recognized previously on Northern blots by the original partial clone obtained via subtractive hybridization (11). 2) In all three RFs, stop codons are found within the first 145 bp of the sequence (RF 1, bp 31–33 and bp 94–96; RF 2, bp 99–101; RF 3, bp 143–145), indicating that the entire 5′ end of any potential ORF lies within the 5′ end of the cDNA. 3) A poly(A) tail of 17 nucleotides is located at the 3′ end, preceded by three AAUAAA polyadenylation consensus hexanucleotides. The significance of the presence of three polyadenylation signals is unclear; however, this region also contains an additional recognition sequence. CACUG (bp 2838–2842), often found near sites of poly(A) addition. 4) A total of 25 separate cDNAs were isolated, based on hybridization to a primer located in the 5′ region; all showed identical restriction patterns, and complete sequence analysis of three full-length clones revealed identity between the cDNAs. Although it is possible that the cDNAs isolated are not full-length, the preponderance of the data suggest that the stannin cDNA encodes a small protein, with the ORF located in the 5′ region of this clone.

The putative stannin ORF is situated such that the 5′ untranslated region is 147 nucleotides in length and the 3′ untranslated region is 2501 nucleotides in length. Although the coding region comprises only a small portion of the total cDNA, as more genes are being cloned it is becoming apparent that this phenomenon is not uncommon (27). Examination of the region beyond the termination codon revealed downstream termination codons in all three RFs (RF 1, bp 463–465; RF 2, bp 534–536; RF 3, bp 503–505), suggesting that the small size of the predicted ORF did not result from creation of a premature termination site through a sequencing error. In addition, analysis of the cDNA sequence for all potential ORFs revealed that the assigned ORF was the largest one present and possessed the most favorable consensus sequence for initiation of translation.

Sequence and *in vitro* translation analysis of a number of full-length and partial stannin cDNA clones provided definitive evidence for the appropriate choice of the ORF. Alignment of various clones according to their common areas of sequence, coupled with the results of *in vitro* translation analysis, revealed which clones possessed regions of the sequence necessary to produce a translation product. With respect to the largest clone isolated, clone 37, the first nucleotide of the I clone occurs at position 605. It had been determined previously that this clone could not generate an *in vitro* translation product and did not contain an ORF within its sequence.[3] Thus, it seemed likely that the ORF start site must occur before position 605, a conclusion verified by *in vitro* translation of an independent clone, clone 6, which also failed to generate an *in vitro* translation product. Relative to clone 37, this clone starts at position 746. Above all, four other independent clones, each containing a region of the sequence before position 605, produced the same translation product. This result indicates that the ORF start site lies within this region and, because two of these clones lack the first 144 nucleotides of the sequence, maps the start site to the region between positions 144 and 605.

The translation products obtained had an estimated molec-

[3] M. L. Billingsley and S. M. Toggas, unpublished observations.

immunoreactivity in all neurons. B, Stannin immunoreactivity in CA3 neurons (400×) (*bar* = 40 μm), showing prominent patches of immunoreactivity in the soma, with some neuronal processes visible. C, Stannin immunoreactivity in CA1 pyramidal cells (100×) (*bar* = 100 μm). D, Stannin immunoreactivity in dentate gyrus (100×) (*bar* = 100 μm), showing staining of the hilus region. E, Stannin immunoreactivity in medial and intermediate subdivisions of entorhinal cortex (100×) (*bar* = 100 μm). F, Staining (400×) (*bar* = 40 μm) of stellate cells in layer 2 and pyramidal cells in layer 3 of entorhinal cortex.

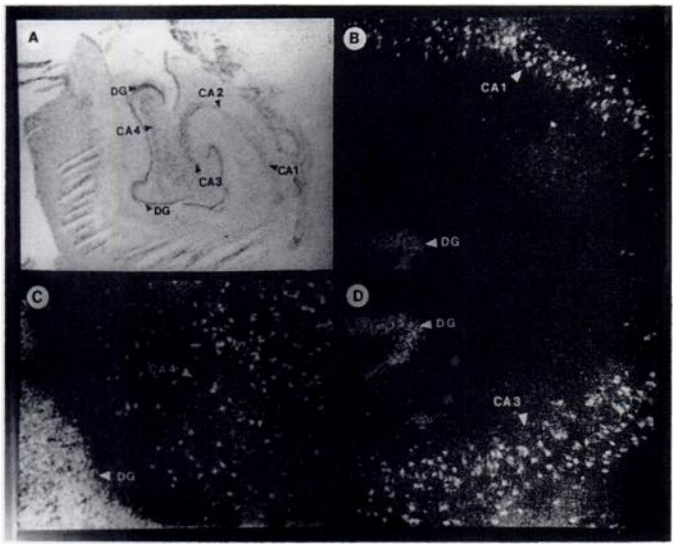


**Fig. 8.** Pattern of *in situ* hybridization of stannin antisense RNA in human hippocampus. Coronal sections (20 μm) of human hippocampus were processed for *in situ* hybridization analysis with radiolabeled stannin antisense RNA, as described in Materials and Methods. Hippocampal sections were exposed for 1–2 weeks (A) and, later, selected slides (B–D) were emulsion coated, exposed for 4–5 weeks, developed, counterstained with cresyl violet, and visualized using dark-field microscopy. A, Autoradiographic image of a human hippocampal section hybridized with the stannin probe (4×). B–D, Regions of human hippocampus seen using dark-field microscopy (40×). *DG*, dentate gyrus; *CA1* to *CA4*, fields of the hippocampus.

ular mass of 15.8 kDa on 10–20% SDS-PAGE gradients, whereas the predicted molecular mass of the protein deduced from the stannin ORF was 10 kDa. We attributed this discrepancy to large amounts of hemoglobin present in the lysate system, which visibly distorted migration of the translation product produced by sense strand mRNAs. Subcloning of the insert of clone 38 into a bacterial expression vector produced an MBP/stannin fusion protein of 52 kDa. Because the reported molecular mass of the MBP is 42 kDa, this result confirms that the ORF encodes a translatable protein of 10 kDa. Finally, antisera directed against the first 15 residues of the putative stannin amino acid sequence also recognized, on Western blots, a protein of 10 kDa in rat hippocampal cytosol. Therefore, on the basis of the aforementioned observations, we are confident that our assignment of the ORF is the correct one.

A study of the tissue distribution of stannin mRNA using Northern blot analysis demonstrated that, in addition to brain, stannin was expressed in kidney and spleen. This finding is of interest because TMT possesses both nephrotoxic and lymphotoxic properties. In rats, TMT-induced nephrotoxicity is manifested as a dose-related cytotoxic effect on proximal tubular epithelial cells. This effect involves cellular vacuolization and brush border attenuation, producing enhanced diuresis and increased urinary pH, 3 days after a single oral dose of TMT at 3, 6, or 10 mg/kg (7). Studies following a single 12.25 mg/kg oral dose demonstrated nephrotoxic effects up to 14 days after administration and found proximal tubular lesions to progress to marked morphologic tubular disruption in the pars recta and medulla, culminating in frank acute renal failure (28). In rats receiving weekly oral doses of 4 mg/kg, hydronephrosis and vacuolar degeneration of renal tubules were noted (29).

In addition, splenic atrophy has been noted after TMT treatment (29). We also observed splenic atrophy 7 days after a single i.p. dose of 8 mg/kg TMT.[4] Lymphotoxic effects of TMT in cultured human peripheral blood lymphocytes included dose-related inhibition of rates of cell division and cell cycle kinetics, along with increased chromosomal aberrations and formation of micronuclei (8). Detection of stannin expression in the thymus gland may be related to lymphotoxicity of TMT; however, thymocytes are more susceptible to the effects of tributyltin than of TMT, although TMT does have some toxic effect on these cells (30). Differences in the toxicity of TMT and tributyltin in thymocytes probably relate to differences in their lipid solubility (5). The presence of stannin mRNA in peripheral tissues affected by TMT further strengthens the hypothesis that stannin may be related to cellular susceptibility to TMT. Moreover, in rats, TMT has not been shown to have toxic effects on liver, heart, or testes (31), tissues in which stannin mRNA was not detected.

Other TMT-sensitive regions containing stannin mRNA were identified via *in situ* hybridization analysis of stannin expression in whole sagittal sections of E15 rats. Strong hybridization in the retinal fields indicated a high level of stannin expression in this area. Similarly, both physiologic and morphologic changes have been reported in the rat retina after TMT intoxication. After a single oral dose of 4–7 mg/kg TMT, there was decreased amplitude of retinal input to the optic tract and visual cortex (32). Morphologic changes seen 3 days after a single oral dose of 6 mg/kg TMT included edematous thickening of the optic fiber layer, as well as degeneration and necrosis in the ganglion cell layer and inner nuclear layer, progressing after 30 days to prominent neuronal loss in these layers and to an overall thinning of the retina (33). Localization of stannin mRNA to autonomic ganglia compares with observations of TMT neurotoxicity in the stellate ganglia. Here, damage appears as severe degeneration, with vacuolization and lysosomal accumulations, and functional effects on muscarinic transmission are seen as a marked reduction in stimulus-induced asynchronous afterdischarges (34).

Hybridization of stannin antisense mRNA to mRNA in trigeminal ganglia may be related to TMT-induced chromalytic changes reported in mesencephalic trigeminal nuclei of the rat; in mice, these changes are accompanied by vacuolar degeneration (35, 36). In addition, TMT has been shown to affect other sensory pathways (33, 37–39).

E15 embryos also exhibited substantial hybridization in the cerebellum and telencephalon. The presence of stannin mRNA in E15 cerebellum is consistent with that reported previously in adult cerebellar granule cells (11). Although the cerebellum is not destroyed by TMT in the rat (6), vacuolation and dense granules were detected in adult rat cerebellum 24 hr after treatment (40). Thoughout development, permanent, dose-related, weight deficits were observed in cerebellum after intoxication with TMT on PND 5 (41). TMT-induced cerebellar dysfunction has also been suggested by behavioral studies (42). Cerebellar destruction by TMT has been reported in other rodent species (43) and, in humans, signs of cerebellar dysfunction ranging from mild nystagmus to severe ataxia were observed in a study of six patients with acute TMT intoxication (44).

Stannin mRNA expression in E15 telencephalon was further

[4] S. M. Toggas, unpublished observations.

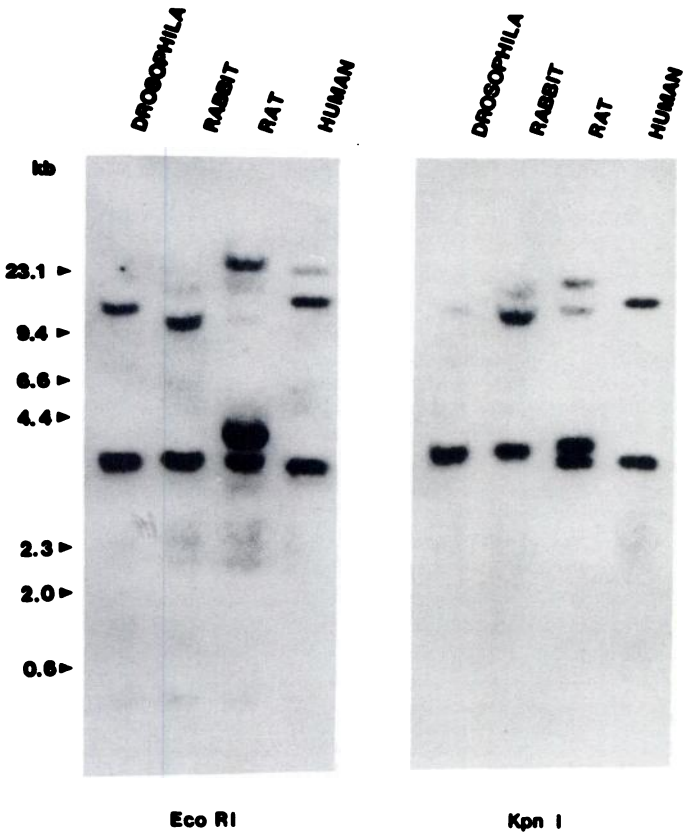


**Fig. 9.** Presence of a gene homologous to rat stannin in human, rabbit, and *Drosophila* DNA. Genomic DNA extracted from *Drosophila*, rabbit spleen, rat brain, and human neuroblastoma cells was digested with either *Eco*RI or *Kpn*I, electrophoresed, and blotted to nylon, using a vacuum. The blot was probed with [$\alpha$-$^{32}$P]dCTP-labeled stannin cDNA and washed under conditions of high stringency (0.1× SSC/0.1% SDS, 65°). Autoradiography was performed at −70° for 20 hr. The strength of the signal obtained indicates a high degree of homology between the probe and the species analyzed.

verified by detection of a 3.0-kb mRNA species on Northern blots of E15 rat brain poly(A)$^+$ mRNA. This species was present at all developmental ages analyzed, a result consistent with the documented neurotoxicity of TMT in the developing rat (41, 42, 45–47).

Immunocytochemical experiments using stannin antipeptide antisera revealed a pattern of localization in hippocampal and other limbic regions, such as entorhinal cortex. Previous *in situ* hybridization experiments demonstrated that the stannin mRNA was localized in the same regions as those expressing immunoreactivity (11). In addition, these neurons are most sensitive to the destructive effects of TMT, suggesting that stannin may play a role in TMT toxicity. Alternatively, stannin may be a marker for damaged neurons. However, patterns of expression of stannin mRNA in kidney, spleen, and sensitive brain regions are provocative, in that these tissues all show selective vulnerability to TMT. Future experiments using heterologous expression of the stannin peptide in TMT-insensitive cells may help determine whether expression of stannin decreases their toxic threshold for TMT.

TMT produces neurotoxic effects in humans in instances of both acute and chronic accidental exposure; behavioral changes occur as memory loss, disorientation, and tonic-clonic seizures, and major pathologic features include necrosis in the hippocampal formation, as well as in amygdala and cerebellum (44, 48). Using *in situ* hybridization analysis of sections of normal human hippocampus, we observed that stannin antisense mRNA hybridized to pyramidal and dentate granule neurons. Other cells in adjacent tissues were unlabeled, further suggesting that expression of stannin occurs in TMT-sensitive cells in human brain.

Southern blot analysis extended characterization of stannin to the genomic level. Results obtained indicate conservation of a gene related to rat stannin in species as diverse as *Drosophila* and human. Because this analysis was performed under stringent conditions, the genomic DNA of each species tested is likely to show considerable homology with the stannin rat brain cDNA probe. Although homology searches of several databases were not fruitful, the presence of a stannin homolog in humans and *Drosophila* suggests that this gene is conserved during evolution and subserves an important function in brain, kidney, and lymphocytes. Molecular genetic analysis in *Drosophila* may allow determination of aspects of stannin function.

There are several caveats that limit the conclusion that there is a direct correlation between stannin expression and TMT sensitivity at this time. First, although stannin is found in many cells that are sensitive to TMT, it is possible that some cells express stannin but show little sensitivity to TMT. However, it is provocative to note that stannin mRNA is found in spleen and kidney, two tissues that are sensitive to TMT. Second, stannin may be a marker protein for a subtype of cells, many of which are sensitive to TMT but which require other factors to show TMT toxicity. In order to address these issues, we are conducting transfection studies with TMT-insensitive cell lines. If stannin expression confers toxicity, then successful transfectants are predicted to show enhanced sensitivity to TMT.

The strategy outlined in this study suggests that molecular biologic approaches afford considerable insight into mechanisms of selective neurotoxicants. Because previous studies failed to outline a plausible mechanism for TMT toxicity, the data presented in this report provide testable hypotheses concerning the role of genetic factors predisposing cells to effects of toxicants. In addition, it is likely that gene products isolated as a result of such strategies play important roles in specialized cellular functions.

**Acknowledgments**

The authors wish to thank Ms. Christine Patanow for expert technical assistance. Thanks also go to Drs. E. Vesell, W. Bartlett, J. P. O'Callaghan, and J. Polli for critical discussion and review of the manuscript.

**References**

1. Zigmond, M. J., and E. M. Stricker. Animal models of Parkinsonism using selective neurotoxins: clinical and basic implications. *Int. Rev. Neurobiol.* **31**:1–79 (1989).
2. Choi, D. W., and S. M. Rothman. The role of glutamate neurotoxicity in hypoxic-ischemic neuronal death. *Annu. Rev. Neurosci.* **13**:171–182 (1991).
3. Perl, T. M., L. Bedard, T. Kokatsky, J. C. Hockin, E. C. D. Todd, and R. S. Remis. An outbreak of toxic encephalopathy caused by eating mussels contaminated with domoic acid. *N. Engl. J. Med.* **322**:1775–1780 (1990).
4. Spencer, P. S., and H. H. Schaumburg. *Experimental and Clinical Neurotoxicology*. Williams and Wilkens, Baltimore (1980).
5. Snoeij, N. J., A. H. Penninks, and W. Seinen. Biological activity of organotin compounds: an overview. *Environ. Res.* **44**:335–353 (1987).
6. Balban, C. D., J. P. O'Callaghan, and M. L. Billingsley. Trimethyltin-induced neuronal damage in the rat brain: comparative studies using silver degeneration stains, immunocytochemistry and immunoassay for neuronotypic and gliotypic proteins. *Neuroscience* **26**:337–361 (1988).
7. Opacka, J., and S. Sparrow. Nephrotoxic effect of trimethyltin in rats. *Toxicol. Lett.* **27**:97–102 (1985).
8. Ghosh, B. B., G. Talukder, and A. Sharma. Cytotoxic effects of trimethylin chloride on human peripheral blood lymphocytes *in vitro*. *Hum. Toxicol.* **8**:349–353 (1989).

9. Brock, T. O., and J. P. O'Callaghan. Quantitative changes in the synaptic vesicle proteins synapsin I and p38 and the astrocyte-specific protein glial fibrillary acidic protein are associated with chemical-induced injury to the rat central nervous system. *J. Neurosci.* **7**:931–942 (1987).
10. O'Callaghan, J. P. Neurotypic and gliotypic proteins as biochemical markers of neurotoxicity. *Neurotoxicol. Teratol.* **10**:445–452 (1988).
11. Krady, J. K., G. A. Oyler, C. D. Balaban, and M. L. Billingsley. Use of avidin-biotin subtractive hybridization to characterize mRNA common to neurons destroyed by the selective neurotoxicant trimethylin. *Mol. Brain Res.* **7**:287–297 (1990).
12. Koenen, M. Recovery of cDNA from agarose gels using liquid nitrogen. *Trends Genet.* **5**:137–138 (1989).
13. Sambrook, J. M., E. F. Fritsch, and T. Maniatis. *Molecular Cloning: A Laboratory Manual*, Ed. 2. Cold Spring Harbor Laboratory, Cold Spring Harbor, NY (1989).
14. Sanger, F., S. Nicklen, and A. R. Coulson. DNA sequencing with chain-terminating inhibitors. *Proc. Natl. Acad. Sci. USA* **74**:5463–5467 (1977).
15. Ausubel, F., R. Brent, R. Kingston, D. Moore, J. Seidman, J. Smith, and K. Struhl. *Current Protocols in Molecular Biology*, Vol. 1. John Wiley and Sons, New York (1989).
16. Hopp, T. P., and K. R. Woods. A computer program for predicting protein antigenic determinants. *Mol. Immunol.* **20**:483–489 (1983).
17. Pearson, W. R., and D. J. Lipman. Improved tools for biological sequence comparison. *Proc. Natl. Acad. Sci. USA* **85**:2444–2448 (1988).
18. Oyler, G. A., G. A. Higgins, R. A. Hart, E. Battenberg, M. L. Billingsley, F. E. Bloom, and M. C. Wilson. The identification of a novel synaptosomal-associated protein, SNAP-25, differentially expressed by neuronal subpopulations. *J. Cell Biol.* **109**:3039–3052 (1989).
19. Laemmli, U. K. Cleavage of structural proteins during the assembly of the head of bacteriophage T4. *Nature (Lond.)* **227**:680–685 (1970).
20. Polli, J. W., M. L. Billingsley, and R. L. Kincaid. Expression of the calmodulin-dependent protein phosphatase, calcineurin, in rat brain: developmental patterns and the role of nigrostriatal innervation. *Dev. Brain Res.* **63**:105–120 (1991).
21. Chirgwin, J. M., A. E. Przybyla, R. J. MacDonald, and W. J. Rutter. Isolation of biologically active ribonucleic acid from sources enriched in ribonuclease. *Biochemistry* **18**:5294–5299 (1979).
22. Cleveland, D. W., M. A. Lopata, R. J. MacDonald, N. J. Cowan, W. J. Rutter, and M. W. Kirshner. Number and evolutionary conservation of $\alpha$- and $\beta$-tubulin and cytoplasmic $\beta$- and $\gamma$-actin genes using specific cloned cDNA probes. *Cell* **20**:95–105 (1980).
23. Wilson, M. C., and G. A. Higgins. *In situ* hybridization. *Neuromethods* **16**:245–291 (1989).
24. Billingsley, M. L., K. R. Pennypacker, C. G. Hoover, and R. L. Kincaid. Biotinylated proteins as probes of protein structure and protein-protein interaction. *BioTechniques* **5**:22–31 (1987).
25. Reynolds, C. P., J. L. Biedler, B. A. Spengler, D. A. Reynolds, R. A. Ross, E. P. Frenkel, and R. G. Smith. Characterization of human neuroblastoma cell lines established before and after therapy. *J. Natl. Cancer Inst.* **76**:375–387 (1986).
26. Kozak, M. An analysis of 5′-noncoding sequences from 699 vertebrate messenger RNAs. *Nucleic Acids Res.* **15**:8125–8148 (1987).
27. Sutcliffe, J. G. mRNA in the mammalian central nervous system. *Annu. Rev. Neurosci.* **11**:157–198 (1988).
28. Robertson, D. G., S.-N. Kim, R. H. Gray, and F. A. de la Iglesia. The pathogenesis of trimethylin chloride-induced nephrotoxicity. *Fundam. Appl. Toxicol.* **8**:147–158 (1987).
29. Brown, A. W., W. N. Aldridge, B. W. Street, and R. D. Verschoyle. The behavioral and neuropathologic sequelae of intoxication by trimethylin compounds in the rat. *Am. J. Pathol.* **97**:59–82 (1979).
30. Aw, T. Y., P. Nicotera, L. Manzo, and S. Orrenius. Tributyltin stimulates apoptosis in rat thymocytes. *Arch. Biochem. Biophys.* **283**:46–50 (1990).
31. Boyer, I. J. Toxicity of dibutyltin, tributyltin, and other organotin compounds to humans and to experimental animals. *Toxicology* **55**:253–298 (1989).
32. Dyer, R. S., W. E. Howell, and W. F. Wonderlin. Visual system dysfunction following acute trimethylin exposure in rats. *Neurobehav. Toxicol. Teratol.* **4**:191–195 (1982).
33. Chang, L. W., and R. S. Dyer. Trimethyltin induced pathology in sensory neurons. *Neurobehav. Toxicol. Teratol.* **5**:673–696 (1983).
34. Christ, D., L. W. Chang, and D. E. McMillan. Neurotoxicological effects of trimethylin on the stellate ganglion. *Neurotoxicol. Teratol.* **11**:453–460 (1989).
35. Chang, L. W., T. M. Tiemeyer, G. R. Wenger, and D. E. McMillan. Neuropathology of trimethylin intoxication. III. Changes in the brain stem neurons. *Environ. Res.* **30**:399–411 (1983).
36. Chang, L. W., G. R. Wenger, D. E. McMillan, and R. S. Dyer. Species and strain comparison of acute neurotoxic effects of trimethylin in mice and rats. *Neurobehav. Toxicol. Teratol.* **5**:337–350 (1983).
37. Crofton, K. M., K. F. Dean, M. G. Menache, and R. Janssen. Trimethyltin effects on auditory function and cochlear morphology. *Toxicol. Appl. Pharmacol.* **105**:123–132 (1990).
38. Fechter, L. D., and L. Carlisle. Auditory dysfunction and cochlear vascular injury following trimethylin exposure in the guinea pig. *Toxicol. Appl. Pharmacol.* **105**:133–143 (1990).
39. Hoeffding, V., and L. D. Fechter. Trimethyltin disrupts auditory function and cochlear morphology in pigmented rats. *Neurotoxicol. Teratol.* **13**:135–145 (1991).
40. Brown, A. W., J. B. Cavanagh, R. D. Verscholye, M. F. Gysbers, H. B. Jones, and W. N. Aldridge. Evolution of the intracellular changes in neurons caused by trimethylin. *Neuropathol. Appl. Neurobiol.* **10**:267–283 (1984).
41. Miller, D. B., and J. P. O'Callaghan. Biochemical, functional and morphological indicators of neurotoxicity: effects of acute administration of trimethylin to the developing rat. *J. Pharmacol. Exp. Ther.* **231**:744–751 (1984).
42. Ruppert, P. H., K. F. Dean, and L. W. Reiter. Developmental and behavioral toxicity following acute postnatal exposure of rat pups to trimethylin. *Neurobehav. Toxicol. Teratol.* **5**:421–429 (1983).
43. Nolan, C. C., A. W. Brown, and J. B. Cavanagh. Regional variations in nerve cell responses to trimethylin intoxication in mongolian gerbils and rats: further evidence for involvement of the Golgi apparatus. *Acta Neuropathol.* **81**:204–212 (1990).
44. Besser, R., G. Kramer, R. Thumler, J. Bohl, L. Gutmann, and H. C. Hopf. Acute trimethylin limbic-cerebellar syndrome. *Neurology* **37**:945–950 (1987).
45. Bouldin, T. W., N. D. Goines, C. R. Bagnell, and M. R. Krigman. Pathogenesis of trimethylin neuronal toxicity: ultrastructural and cytochemical observations. *Am. J. Pathol.* **104**:237–249 (1981).
46. Mushak, P., M. R. Krigman, and R. B. Mailman. Comparative organotin toxicity in the developing rat: somatic and morphological changes and relationship to accumulation of total tin. *Neurobehav. Toxicol. Teratol.* **4**:209–215 (1982).
47. Paule, M. G., K. Reuhl, J. J. Chen, S. F. Ali, and W. Slikker, Jr. Developmental toxicology of trimethylin in the rat. *Toxicol. Appl. Pharmacol.* **84**:412–417 (1986).
48. Ross, W. D., E. A. Emmett, J. Steiner, and R. Tureen. Neurotoxic effects of occupational exposure to organotins. *Am. J. Psychiatry* **138**:1092–1095 (1981).


**Send reprint requests to:** Dr. Melvin L. Billingsley, Department of Pharmacology, Milton S. Hershey Medical Center, Pennsylvania State University College of Medicine, P.O. Box 850, Hershey, PA 17033.